AIAA 2001-1427

AN INTEGRATED TRIM AND STRUCTURAL DESIGN PROCESS FOR ACTIVE AEROELASTIC WING TECHNOLOGY

P. Scott Zink*, Daniella E. Raveh†, Dimitri N. Mavris‡
Aerospace Systems Design Laboratory
School of Aerospace Engineering
Georgia Institute of Technology, Atlanta, GA 30332-0150

Abstract

A new method for concurrent trim and structural optimization of Active Aeroelastic Wing technology is presented. The new process treats trim optimization and structural optimization as an integrated problem in the same mathematical formulation, in which control surface gear ratios are included as design variables in a standard structural optimization algorithm. This new approach is in contrast to most of the existing AAW design processes in which structural optimization and trim optimization have separate objectives and are performed in an iterative, sequential manner. The new integrated AAW design process is demonstrated on a lightweight fighter type aircraft and compared to a sequential AAW design process. For this demonstration, the integrated process converges to a lower weight, and offers an advantage over the sequential process in that optimization is performed in one continuous run, whereas the sequential approach requires pausing and restarting the structural optimization to allow for trim optimization.

Introduction

An emerging and promising technology for addressing the problem of adverse aeroelastic deformation, such as control surface reversal, is Active Aeroelastic Wing (AAW) technology. It has recently been a key area of study for both the government and industry[1,2] and is defined by Pendleton et. al., as "a multidisciplinary, synergistic technology that integrates air vehicle aerodynamics, active controls, and structures together to maximize air vehicle performance"[3]. AAW technology exploits the use of leading and trailing edge control surfaces to aeroelastically shape the wing, with the resulting aerodynamic forces from the flexible wing becoming the primary means for generating control power. With AAW, the control surfaces then act mainly as tabs and not as the primary sources of control power as they do with a conventional control philosophy. As a result, wing flexibility is seen as an advantage rather than a detriment since the aircraft can be operated beyond reversal speeds and still generate the required control power for maneuvers. Hence, there is potential for significant reductions in structural weight and actuator power.

Figure 1 illustrates conceptually the differences between AAW technology and a conventional control approach for a rolling maneuver. The hypothetical example shows the cross section of two wings deforming due to aeroelastic effects. The upper wing, employing AAW technology, is twisting in a positive way with the use of both leading and trailing edge surfaces, while the conventionally controlled, lower wing, which uses only the trailing edge surface, is twisting in a negative way[4]. This adverse twist due to the deflection of the trailing edge surface is associated with reduced control surface effectiveness and control surface reversal, in which the increase in camber due to the deflection of the surface is offset by the negative twist of the wing[5].

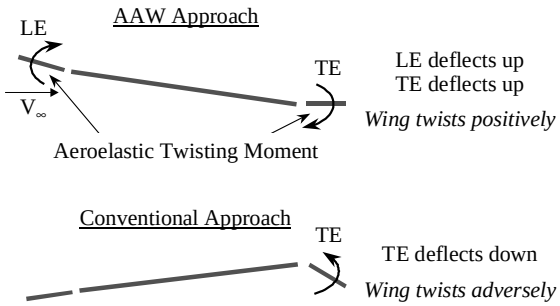

Figure 1 - AAW Technology vs. Conventional Control

Since AAW technology is multidisciplinary in nature, structural design using the technology necessarily requires detailed information about the vehicle structures, aerodynamics, and controls, and in particular, is heavily dependent on control law design. Thus, there is a need for an integrated AAW design process in which the structure and control laws are optimized concurrently.

In consideration of AAW technology's use of redundant control surfaces, an important constituent of the technology are *control surface gear ratios* which dictate how one control surface deflects with respect to a single basis surface. Two gear ratio scenarios are illustrated in Figure 2 in which the deflections of the

---

* Ph.D. Candidate, Student Member AIAA
† Research Engineer II, Member AIAA
‡ Boeing Chair in Advanced Aerospace Systems Analysis, Associate Fellow AIAA

leading edge inboard (LEI), leading edge outboard (LEO), and trailing edge inboard (TEI) surfaces are linearly dependent on the deflection of the trailing edge outboard surface (TEO). This concept is also referred to as control surface blending and for the purposes of this research constitute the control laws.

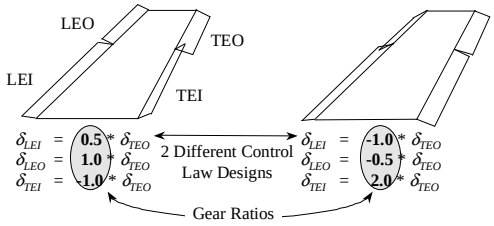

Figure 2 – Gear Ratio Illustration

The *AAW design process* refers to the concurrent optimization of the structure and gear ratios. Structural optimization refers to the sizing of structural elements (e.g., skin thickness, spar thickness) to minimum weight, subject to stress, aeroelastic constraints, etc. Trim optimization refers to the process of selecting the gear ratios, or control surface deflection angles, that trim the aircraft to a prescribed maneuver while optimizing a certain objective function within actuator limits. The need for trim optimization is due to AAW technology's use of redundant control surfaces, which means that the static aeroelastic trim equations cannot be solved in a closed form manner. Much research has been done in this area, where References [6], [7], [8], [9], and [10] discuss several approaches by which this problem has been tackled.

The literature dealing with the AAW design process is more limited, and most of the methods that have been developed are those in which trim optimization and structural optimization are separate optimization problems performed in a sequential manner. For the purposes of this paper this type of AAW design process is referred to as a *sequential* AAW design process. Zillmer[11,12] developed such an approach. In this case, trim optimization, performed using a Rockwell-developed code ISMD (Integrated Structure/Maneuver Design), is embedded in an iterative process with NASTRAN[13]. The control surface deflections, in ISMD, are optimized to minimize a composite function of stress, induced drag, and buckling load. The maneuver loads resulting from the optimized control surface deflections of ISMD are transferred to NASTRAN which then optimizes the structure to minimum weight. NASTRAN then passes stability derivatives and sensitivity information of the current structural design to ISMD for another trim optimization. This process repeats itself until the wing weight converges.

Another example, in the literature, of a sequential AAW design process is found in Love et al.[9] In this case, the trim optimization module, in which the deflection of the control surfaces are optimized to minimize user-defined component loads (e.g. root bending moment, hinge moment), was placed within the structural optimization loop of ASTROS (Automated Structural Optimization System)[14], a finite element-based structural optimization code. For each iteration in the structural optimization, the control surface deflections for the current structural design are optimized. Then with these new deflections the structural optimizer proceeds to take another step, pauses again for trim optimization, and so on, until the structural optimization objective, wing weight, converges.

Zink et al.[15,16] applied the techniques of Reference [9] in a design study of a generic lightweight fighter concept employing AAW technology, with four wing control surfaces and a horizontal tail. Trim optimization was performed for antisymmetric (rolling) and symmetric maneuvers. The trim optimization problem for the symmetric maneuver was posed as a minimization of root bending moment (RBM), whereas a summation of the wing hinge moments was the objective for the antisymmetric maneuvers. It was solved using a gradient-based optimization algorithm. The intention was that trim and structural optimization would be repeated iteratively. However, only the first step was demonstrated, as trim optimization was performed only once on the starting structural design. As an evolution of the work in References [15] and [16], and in addressing some of the problems encountered in that study, a new sequential AAW design process was developed that employs the simplex method[17] for trim optimization. This new sequential process is reviewed briefly in the current work and documented in detail in Reference [10].

Miller[6] proposed an AAW design process in which the thickness of the structural elements and the control surface deflections were simultaneous design variables in an integrated optimization problem. The objective of this approach was the minimization of weight, subject to trim balance requirements, stress constraints, and buckling load constraints. This approach represents a diversion from the previous AAW design processes as, in this case, trim optimization and structural optimization are not separate problems.

In the current research, a similar AAW design process is developed in which trim and structural optimization are posed as an integrated problem in the same mathematical formulation. However, in this approach, the control surface gear ratios, rather than their deflections, are added as design variables to the structural optimization. Additionally, hinge moments are included in the optimization problem as constraints.

The possible advantages of the integrated AAW design process include better solution convergence and lower weight structural designs. Its development and comparison with the sequential AAW design process of Reference [10] is the goal of the current effort.

Methodology

Integrated AAW Design Process

The formulation of the integrated AAW design process is as follows:

Minimize: *Weight*

Subject to: *Material Strain Allowables*

Control Surface Travel Limits

$-30^o \le \delta_{LEI_j} \le 5^o$, $-30^o \le \delta_{LEO_j} \le 5^o$,

$-30^o \le \delta_{TEI_j} \le 30^o$, $-30^o \le \delta_{TEO_j} \le 30^o$,

$-30^o \le \delta_{HT_j} \le 30^o$

Hinge Moment Constraints

$-3.0*10^5 \le HM_{LEI_j} \le 3.0*10^5$,

$-1.0*10^5 \le HM_{LEO_j} \le 1.0*10^5$,

$-1.5*10^5 \le HM_{TEI_j} \le 1.5*10^5$,

$-5.0*10^4 \le HM_{TEO_j} \le 5.0*10^4$ (lb-in)

$j = 1,\ldots, nm$

Design Variables:

$t_1,\ldots t_n, g_1,\ldots g_m$

n: number of thickness variables

m: number of gear ratio design variables

where t_i are the traditional structural design variables, g_i are the new gear ratio design variables, HT is the horizontal tail, HM_i are the control surface hinge moments, *nm* is the number of maneuvers being considered, and δ_i are the control surface deflections. The control surface travel limits and hinge moment limits are based on typical allowables for modern fighter aircraft.

The optimization problem above is implemented in modal-based ASTROS, which provides efficient and accurate finite element-based static aeroelastic analysis and optimization[18,19]. The optimization is based on the hybrid modal approach in which trim is computed in modal coordinates, while stress analysis is performed in discrete coordinates for greater accuracy. The optimization problem is solved by the Modified Method of Feasible Directions[20] algorithm. At the heart of the modal approach is the representation of the discrete displacements as a linear combination of the free aircraft low frequency modes of vibration which are then used to create the generalized stiffness, mass, and force matrices which comprise the static aeroelastic equation. Modal-based static aeroelastic equations are assembled for each maneuver to which the structure and gear ratios are designed and are then solved to evaluate the above constraints. In addition, the static aeroelastic equation is used to derive analytical sensitivities of the constraints with respect to the design variables, as opposed to numerical sensitivities calculated through finite differencing. Use of the modal approach, along with analytic sensitivities, then reduces the size of the analysis and optimization problem significantly.

Although the optimal weight is not an explicit function of the gear ratios, the stress/strain, and hinge moment constraints are, and thus sensitivities of these constraints with respect to each of the gear ratios of interest for each maneuver are required. Analytical sensitivities of these constraints have been derived for the static aeroelastic equation in modal coordinates. The derivation of the sensitivities of the objective and constraints with respect to the thickness variables, in addition to solution of the modal-based static aeroelastic equation for constraint evaluation, are provided in Reference [21] and will not be repeated here.

Gear Ratio Sensitivities

The basic equation for the static aeroelastic analysis of a maneuvering aircraft by the finite element method in discrete coordinates is[22]:

$$[[K] - q[AICS]]\{u\} + [M][\phi_r]\{\ddot{u}_r\} = [P]\{\delta\} \qquad (1)$$

where $[K]$ is the stiffness matrix, $[AICS]$ is the aerodynamic influence coefficients matrix transformed to the structural degrees of freedom, $\{u\}$ are the displacements and rotations at the structural nodes, $[M]$ is the mass matrix, $[\phi_r]$ are the rigid body modes of the free aircraft, $\{\ddot{u}_r\}$ is a vector of rigid body accelerations, $[P]$ is a matrix of the rigid aerodynamic force coefficients due to aerodynamic trim parameters, q is the dynamic pressure, and $\{\delta\}$ is the aerodynamic trim parameter values (e.g., angle of attack, control surface deflection, roll rate).

Equation (1) is transformed to modal coordinates by assuming that the displacements, $\{u\}$, are a linear combination of the low frequency modes of vibration, as given by:

$$\{u\} = \begin{bmatrix}\phi_r & \phi_e\end{bmatrix}\begin{Bmatrix}\xi_r \\ \xi_e\end{Bmatrix} \qquad (2)$$

where $[\phi_r \quad \phi_e]$ is the modal matrix comprised of the rigid body modes, $[\phi_r]$, and a subset of the elastic modes, $[\phi_e]$. $\{\xi_r\}$ are the rigid body modal displacements, and $\{\xi_e\}$ are the elastic modal displacements. Substitution of Equation (2) into Equation (1) and pre-multiplication of Equation (1) by the transpose of the modal matrix yields the static aeroelastic equation in modal coordinates[21]:

$$\begin{bmatrix} -qGAIC_{rr} & -qGAIC_{re} \\ -qGAIC_{er} & GK_{ee} - qGAIC_{ee} \end{bmatrix} \begin{Bmatrix} \xi_r \\ \xi_e \end{Bmatrix} + \begin{bmatrix} M_{rr} \\ M_{er} \end{bmatrix} \{\ddot{\xi}_r\} = \begin{bmatrix} PA_r \\ PA_e \end{bmatrix} \{\delta\} \tag{3}$$

Considering that with AAW technology $\{\delta\}$ contains a redundant number of aerodynamic trim parameters, a gearing matrix ($\{\delta\} = [G]\{\delta_I\}$) is introduced to the right hand side of Equation (3). This gearing matrix, $[G]$, contains the gear ratios, g_i, and relates the redundant (dependent) trim parameters to the determinate (independent) ones, $\{\delta_I\}$. The number of independent trim parameters equals the number of rigid body degrees of freedom. Taking the derivative of Equation (3) (where $[GPA] = [PA][G]$) with respect to the i^{th} gear ratio results in the following:

$$\begin{bmatrix} -qGAIC_{rr} & -qGAIC_{re} \\ -qGAIC_{er} & GK_{ee} - qGAIC_{ee} \end{bmatrix} \begin{Bmatrix} DXIG_r \\ DXIG_e \end{Bmatrix}_i + \begin{bmatrix} M_{rr} \\ M_{er} \end{bmatrix} \{DUDG_r\}_i = \begin{bmatrix} GPA_r \\ GPA_e \end{bmatrix} \{DDELG\}_i + \begin{bmatrix} DGPAG_r \\ DGPAG_e \end{bmatrix}_i \{\delta_I\} \tag{4}$$

where:

$$\{DXIG_r\}_i = \frac{\partial\{\xi_r\}}{\partial g_i} \qquad \{DXIG_e\}_i = \frac{\partial\{\xi_e\}}{\partial g_i}$$

$$\{DUDG_r\}_i = \frac{\partial\{\ddot{\xi}_r\}}{\partial g_i} \qquad \{DDELG\}_i = \frac{\partial\{\delta_I\}}{\partial g_i}$$

$$[DGPAG_r]_i = \frac{\partial[GPA_r]}{\partial g_i} \qquad [DGPAG_e]_i = \frac{\partial[GPA_e]}{\partial g_i}$$

Combining the left hand terms of Equation (4):

$$\begin{bmatrix} -qGAIC_{rr} & -qGAIC_{re} & M_{rr} \\ -qGAIC_{er} & GK_{ee} - qGAIC_{ee} & M_{er} \end{bmatrix} \begin{Bmatrix} DXIG_r \\ DXIG_e \\ DUDG_r \end{Bmatrix}_i = \begin{bmatrix} GPA_r \\ GPA_e \end{bmatrix} \{DDELG\}_i + \begin{bmatrix} DGPAG_r \\ DGPAG_e \end{bmatrix}_i \{\delta_I\} \tag{5}$$

Equation (5) is a system of $n_r + n_e$ equations with $2n_r + n_e$ unknown sensitivities, where n_r and n_e are the number of rigid body modes and elastic modes, respectively. $\{\delta_I\}$ is known as we are differentiating about a known static aeroelastic equilibrium condition, and the sensitivity terms, $[DGPAG_r]_i$ and $[DGPAG_e]_i$, are known, as well, as they are the columns of $[PA_r]$ and $[PA_e]$, respectively, that correspond to the i^{th} gear ratio. For example, if the rigid body accelerations, $\{\ddot{\xi}_r\}$, are defined by the user for a specific maneuver, then $\{DUDG_r\}_i$ is zero, since the accelerations are constant. In this case, then, the unknown sensitivities are the n_e elements of $\{DXIG_e\}_i$, the n_r elements of $\{DXIG_r\}_i$, and the n_r elements of $\{DDELG\}_i$, which are more unknowns than equations available to solve them. An additional equation is introduced which is based on the assumption that the displacement, $\{u\}$, does not change the location of the center of gravity or orientation of the mean axis system, which defines the alignment of the aircraft moments of inertia[23]. This assumption leads to the rigid body modes, $[\phi_r]$, being orthogonal to the displacement vector, $\{u\}$, with respect to the mass matrix, which expressed in modal coordinates leads to the following equation:

$$[M_{rr}]\{\xi_r\} + [M_{er}]^T\{\xi_e\} = \{0\} \tag{6}$$

Differentiating with respect to g_i, Equation (6) becomes:

$$[M_{rr}]\{DXIG_r\}_i + [M_{er}]^T\{DXIG_e\}_i = \{0\} \tag{7}$$

Solving for $\{DXIG_r\}_i$:

$$\{DXIG_r\}_i = -[M_{rr}]^{-1}[M_{er}]^T\{DXIG_e\}_i \tag{8}$$

Substituting Equation (8) into Equation (5), Equation (5) becomes:

$$\begin{bmatrix} q[GAIC_{rr}][M_{rr}]^{-1}[M_{er}]^T - q[GAIC_{re}] & [M_{rr}] \\ q[GAIC_{er}][M_{rr}]^{-1}[M_{er}]^T + [GK_{ee}] - q[GAIC_{ee}] & [M_{er}] \end{bmatrix} \times \begin{Bmatrix} DXIG_e \\ DUDG_r \end{Bmatrix}_i = \begin{bmatrix} GPA_r \\ GPA_e \end{bmatrix} \{DDELG\}_i + \begin{bmatrix} DGPAG_r \\ DGPAG_e \end{bmatrix}_i \{\delta_I\} \tag{9}$$

Equation (9) reflects a set of $n_r + n_e$ equations with $n_r + n_e$ unknowns, which are the elements of $\{DDELG\}_i$ and $\{DXIG_e\}_i$. Taking the 2nd row of Equation (9) and solving for $\{DXIG_e\}_i$:

$$\{DXIG_e\}_i = [GKA_{ee}]^{-1} \begin{pmatrix} [GPA_e]\{DDELG\}_i - \\ [M_{er}]\{DUDG_r\}_i + \\ [DGPAG_e]_i\{\delta_I\} \end{pmatrix} \tag{10}$$

where:

$$[GKA_{ee}] = q[GAIC_{er}][M_{rr}]^{-1}[M_{er}]^T + [GK_{ee}] - q[GAIC_{ee}] \tag{11}$$

Substituting Equation (10) into the 1st row of Equation (9), and rearranging terms, the first row of Equation (9) can be written as:

$$[LHSA]\{DUDG_r\}_i = [RHSA]\{DDELG\}_i + [DRHSG]_i\{\delta_I\} \tag{12}$$

where:

$$[LHSA] = [M_{rr}] + q[GAIB_{re}][GKA_{ee}]^{-1}[M_{er}] \quad (13)$$

$$[RHSA] = [GPA_r] + q[GAIB_{re}][GKA_{ee}]^{-1}[GPA_e] \quad (14)$$

$$[DRHSG]_i = [DGPAG_r]_i + q[GAIB_{re}][GKA_{ee}]^{-1}[DGPAG_e]_i \quad (15)$$

$$[GAIB_{re}] = [GAIC_{re}] - [GAIC_{rr}][M_{rr}]^{-1}[M_{er}]^T \quad (16)$$

Equation (12) is used to solve for the n_r unknown trim *sensitivities*, $\{DDELG\}_i$. These sensitivities are calculated through algebraic manipulation of Equation (12), and are substituted into Equation (10) to find the elastic modal displacement sensitivities, $\{DXIG_e\}_i$. The rigid modal displacement sensitivities $\{DXIG_r\}_i$ are then estimated by substitution of $\{DXIG_e\}_i$ into Equation (8). Once the sensitivities for the modal displacements are found, the sensitivities for stress and strain can be easily calculated by multiplying the modal displacement sensitivities by the fixed strain-displacement, stress-displacement transformation matrices.

Sensitivity of Dependent Surface Deflections

The control surface deflection constraints required significant modification to the ASTROS solution sequence. In the unmodified version of ASTROS, the independent control surface deflections can be directly constrained, and since the gear ratios remain fixed in a conventional structural optimization, the dependent surface deflections could be constrained, as well, through the constraint on the independent surface. However, with the integrated AAW design process, in which the gear ratios are changing with every iteration, the dependent surfaces cannot be directly constrained. In fact, this was a limitation of a previous version of the integrated process as presented in Reference [24]. As a result, a new capability was added so that the dependent surface deflections could be directly constrained. This required the addition of a new constraint type and sensitivity calculation of the dependent surface deflection with respect to the gear ratios and structural design variables.

The deflection of a dependent control surface (δ_j) is given by the following equation:

$$\delta_j = g_j \cdot \delta_I \quad (17)$$

where g_j is its corresponding gear ratio and δ_I is the independent surface to which it is geared, whose deflection is found through solution of the static aeroelastic equation of motion (Equation 3). The sensitivity, then, of the dependent surface deflection with respect to a gear ratio design variable (g_i) is calculated by:

$$\frac{\partial \delta_j}{\partial g_i} = \begin{cases} g_j \cdot \dfrac{\partial \delta_I}{\partial g_i} & i \neq j \\ \delta_I + g_j \cdot \dfrac{\partial \delta_I}{\partial g_i} & i = j \end{cases} \quad (18)$$

where $\partial\delta_I/\partial g_i$ is found from $\{DDELG\}_i$ in Equation (12).

The sensitivity of the dependent surface deflection with respect to a structural design variable (t_i) is given by:

$$\frac{\partial \delta_j}{\partial t_i} = g_j \cdot \frac{\partial \delta_I}{\partial t_i} \quad (19)$$

Sensitivity of Aerodynamic Loads

The total aerodynamic loads (including those due to flexibility effects) on the aerodynamic grid are[21]:

$$\{P_k\} = q\left([AIRFRCG]\{\delta_I\} + [AIC]\left([GGS_{ke}]\{\xi_e\} + [GGS_{kr}]\{\xi_r\}\right)\right) \quad (20)$$

where [*AIRFRCG*] are the rigid aerodynamic force coefficients due to unit deflection of the independent trim parameters in the aerodynamic degrees of freedom, and $[GGS_{ke}]$ and $[GGS_{kr}]$ are spline matrices transforming displacements in modal coordinates to displacements in the aerodynamic grid.

Differentiating Equation (20) with respect to g_i, Equation (20) becomes:

$$\{DPKG\}_i = q\left([AIRFRC]\{DDELG\}_i + [DAIRFRCG]_i\{\delta_I\} + [AIC]\left([GGS_{ke}]\{DXIG_e\}_i + [GGS_{kr}]\{DXIG_r\}_i\right)\right) \quad (21)$$

where $\{DDELG\}_i$, $\{DXIG_e\}_i$, $\{DXIG_r\}_i$ are defined previously,

$$\{DPKG\}_i = \frac{\partial\{P_k\}}{\partial g_i}$$

and $[DAIRFRCG]_i$ are the aerodynamic forces due to a unit deflection of the control surface associated with the i^{th} gear ratio. The sensitivities of the hinge moment constraints can then be found by multiplying $\{DPKG\}_i$ by an appropriate transformation matrix which represents the moment arm and remains fixed

throughout the optimization. These sensitivities are also required for discrete stress analysis in the hybrid modal approach[21]. The analytical sensitivities presented here have been verified by comparing them with sensitivities estimated by numerical differentiation (using finite differences).

Sequential AAW Design Process

The sequential AAW design process of Reference [10] is performed by iterating between trim optimization, by the simplex method in MATLAB[25], and structural optimization by modal-based ASTROS, as presented in Figure 3. For each structural optimization iteration, the control surface deflections for the current structural design are optimized (represented by the MATLAB block). Then, these new control surface deflections are converted to gear ratios and passed to ASTROS which reassembles the static aeroelastic equations with the new gear ratios. ASTROS then performs structural redesign to reduce weight using the optimization algorithm of Reference [20]. After the structural optimization step, the aeroelastic equations for the new structural design are assembled, and the appropriate stability derivatives, trim objective and constraint sensitivities are calculated in ASTROS and then output to trim optimization. This process repeats itself until the structural optimization objective, wing weight, is converged.

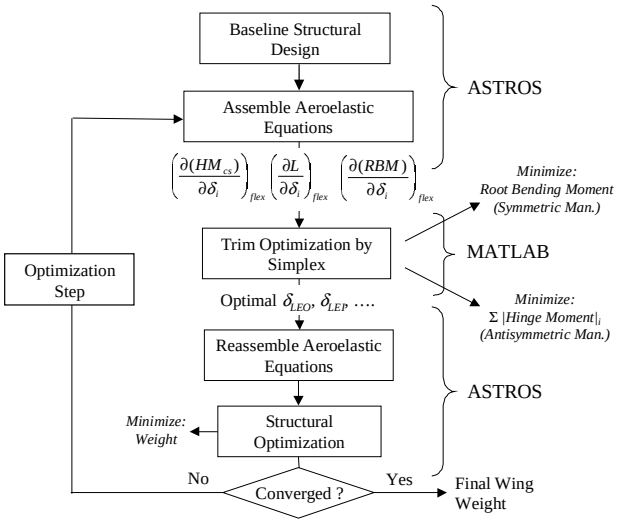

Figure 3 – Sequential AAW Design Process[10]

Trim optimization, for the symmetric maneuvers of Reference [10], is posed as a minimization of root bending moment (*RBM*), where the wing control surfaces are used to tailor the load distribution and provide load relief at the wing root, thus ultimately reducing wing weight. For the antisymmetric maneuvers, the objective of trim optimization is to minimize a summation of the absolute value of each control surface hinge moment, as given by:

$$\text{Minimize: } |HM_{LEI}| + |HM_{LEO}| + |HM_{TEI}| + |HM_{TEO}|$$

This objective can be converted to linear programming form[26] by a simple transformation of the optimization problem. The details of this are reported in Reference [10].

Numerical Example

Structural and Aerodynamic Model

The structural model of the aircraft used both in this research and in Reference [10] is shown in Figure 4. It is an ASTROS preliminary design finite element model of a lightweight composite fighter aircraft with 4 wing control surfaces (2 trailing edge, 2 leading edge) and a horizontal tail[18,27]. It corresponds to a wing with an aspect ratio of 3.0, a total planform area of 330 ft^2, a taper ratio of 20 %, a leading edge sweep of 38.7°, and a thickness ratio of 3%. The skin of the wing is made up of 4 composite plies with orientations of 0°, ± 45°, and 90°, where the thickness of the –45° and +45° plies are constrained to be equal. The number of modes that serve as generalized coordinates for both symmetric and antisymmetric boundary conditions is 35.

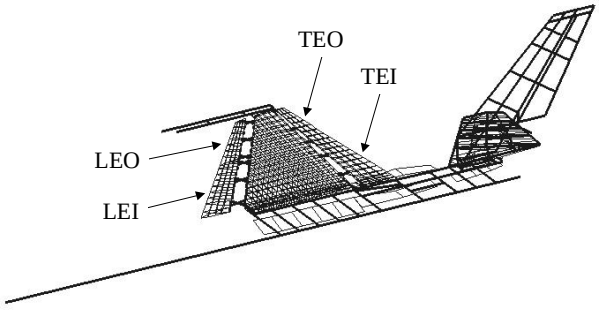

Figure 4 - Structural Model of Generic Fighter

The aerodynamic model is shown in Figure 5. It is a flat-panel Carmichael[28] model containing 143 vertical panels and 255 horizontal panels. It also contains paneling for the four wing control surfaces and horizontal tail to coincide with the control surfaces on the structural model. Carmichael aerodynamic influence coefficients are produced for two Mach numbers, 0.95 and 1.2, for both symmetric and antisymmetric maneuvers[29].

The structural design variables (t_i) in the AAW design process are the layer thickness of the composite skins. The number of structural design variables is 78 due to physical linking of the skin elements. Internal structure and carry-through structure remain fixed. Table 1 shows the maneuver conditions and strength

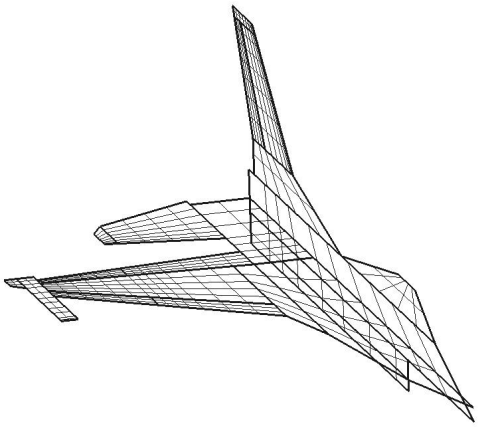

Figure 5- Aerodynamic Model of Generic Fighter

constraints to which the structure is designed for both the sequential and integrated AAW design processes. While a realistic fighter design requires the consideration of asymmetric 3 degree of freedom rolling pull-out maneuvers, this study is limited to pure symmetric and antisymmetric maneuvers for simplicity. To account for this, the strength constraints of the antisymmetric maneuvers were lowered, acknowledging that additional strain would result from the symmetric component of the asymmetric maneuver. In addition to the strength constraints, for the integrated approach, hinge moment constraints and control surface travel limits are also included, as discussed in a previous section.

Table 1 - Maneuver Conditions and Design Constraints

Maneuver Condition	Design Constraint
1) Mach 0.95, 10,000 ft. 9g Pull Up	fiber strain: 3000 με tension 2800 με compression
2) Mach 1.20, Sea Level -3g Push Over	fiber strain: 3000 με tension 2800 με compression
3) Mach 1.20, Sea Level Steady State Roll = 100^{O}/s	fiber strain: 1000 με tension 900 με compression
4) Mach 0.95, 10,000 ft. Steady State Roll = 180^{O}/s	fiber strain: 1000 με tension 900 με compression

The gear ratio design variables (g_i) of the integrated process, for each maneuver, are shown in Table 2, along with the independent surface for each maneuver to which the dependent surfaces are geared. For example, the variable, g_{LEI3}, is the ratio of the deflection of the LEI surface to the deflection of the LEO surface for the supersonic roll. The horizontal tail was selected as the independent surface for Maneuvers 1 and 2, since it has historically been the primary control surface for symmetric trim. The LEO surface was selected for Maneuver 3, because it is the most effective surface at supersonic conditions, at which point both trailing edge surfaces experience control reversal. For Maneuver 4, the TEO surface is the independent surface, since it is the most effective roll control surface at subsonic speeds.

Table 2 – Gear Ratio Design Variables

	Independent Surface	Gear Ratio Design Variables
Maneuver 1	HT	g_{LEI1}, g_{LEO1}, g_{TEI1}, g_{TEO1}
Maneuver 2	HT	g_{LEI2}, g_{LEO2}, g_{TEI2}, g_{TEO2}
Maneuver 3	LEO	g_{LEI3}, g_{TEI3}, g_{TEO3}
Maneuver 4	TEO	g_{LEI4}, g_{LEO4}, g_{TEI4}

Results

The integrated AAW design process, here proposed, has been implemented in modal-based ASTROS and demonstrated on the previously discussed model. It is compared with the sequential AAW design process, discussed in detail in Reference [10]. As shown in Table 3, a comparison of the optimal weights by each approach reveals that the integrated approach converges to a significantly lower (15 % less) weight. The weight presented here corresponds only to those structural elements that were designed, namely the wing box skins. The integrated approach converged to its solution in 10 iterations, while the sequential approach took 6 iterations.

Table 3 – Final Weights for each AAW Design Process

AAW Design Process	Weight (lb)
Sequential	292.3
Integrated	248.0

Figure 6 shows a comparison of the optimal total upper surface skin thickness of the wing box by the integrated and sequential AAW design processes. The thickness displayed is a summation of the optimal thickness of all four composite plies, and the shaded regions show those zones of the wing box skins that were linked together as single design variables for the purposes of reducing the size of the design task. A cursory examination of both figures reveals, as expected, that thinner skins result from the integrated approach. In particular, one observes rather dramatic

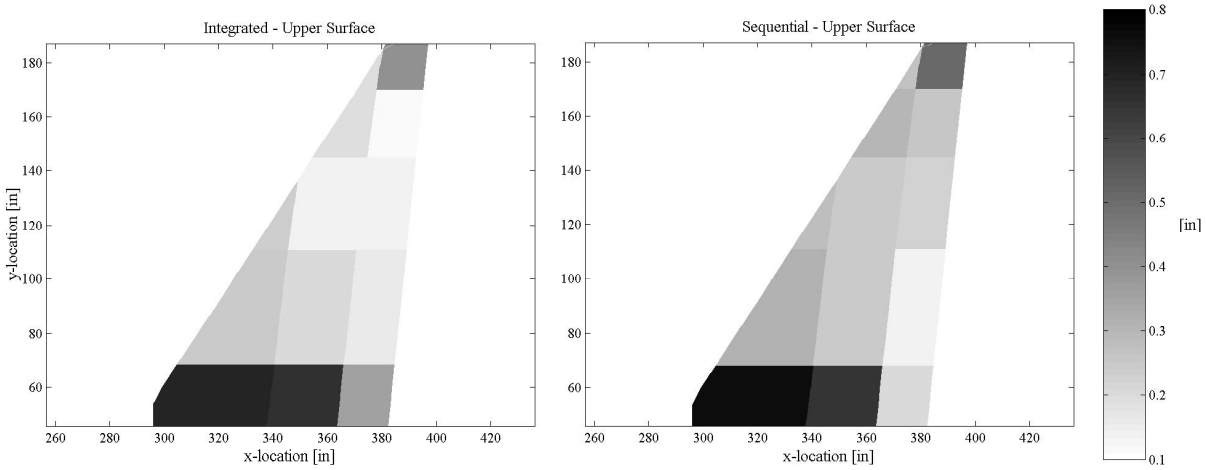

Figure 6 - Optimal Total Skin Thickness (Upper Surface)

reductions in skin thickness in the mid and outboard sections of the wing. However, at the wing roots the two approaches result in comparable skin thickness. This is most likely attributed to the sequential approach's minimization of RBM for the subsonic pull-up maneuver which is the maneuver that typically sizes the inboard part of the wing. Minimization of the bending moment at the wing root dramatically relieves internal load in this region, but it does not necessarily relieve load as much in other parts of the wing. Hence, one observes that the sequential approach with the minimization of RBM as the trim optimization objective results in comparable skin thickness at the wing root but fails to compete with the integrated approach in other parts of the wing. This leads to a beneficial property of the integrated approach which is that it provides weight savings to all parts of the wing by acting at the element level to relieve strain, whereas with the sequential approach, dependent upon the choice of the trim optimization objective, weight savings tend to be more concentrated in local areas. Similar trends in the optimal skin thickness between the integrated and sequential AAW design process were found on the lower surface, as well, which for length considerations are not presented here.

Figure 7 shows the iteration history of the gear ratio design variables by both the sequential and integrated AAW design processes, along with the final control surface deflections, for the subsonic pull-up. The control surface deflections are simply the trimmed

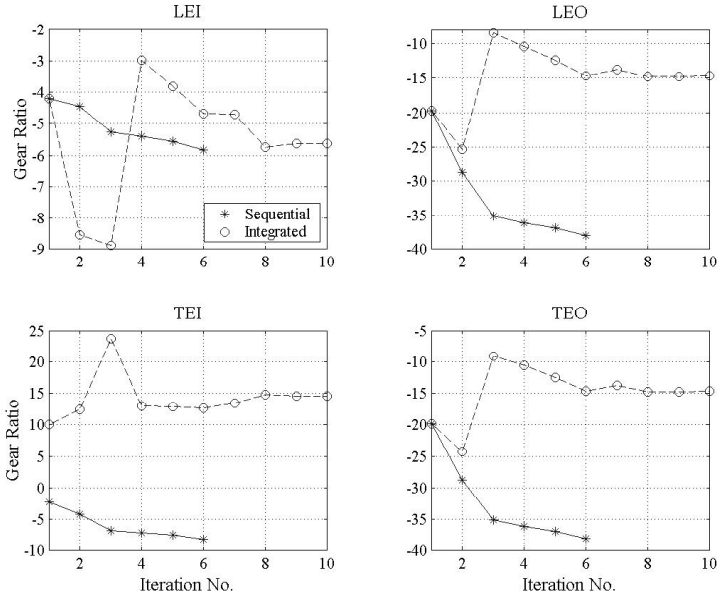

Final Control Surface Deflections

	Sequential	Integrated
δ_{LEI}	-4.609º	-11.522º
δ_{LEO}	-30.056º	-30.000º
δ_{TEI}	-6.446º	29.859º
δ_{TEO}	-30.056º	-30.000º
δ_{HT}	0.790º	2.045º
α	11.751º	9.312º

Figure 7 - Gear Ratio History – Maneuver 1

values of the independent surface (in this case the horizontal tail) multiplied by the corresponding gear ratios. Experience showed that the best starting values for the gear ratio design variables were those as found by trim optimization of the sequential approach for the baseline (i.e., starting) structural design. An exception to this guideline is found in the TEI surface of Figure 7, in which the best starting value for g_{TEI1} was +10.0 (instead of –2.26 as in the sequential approach).

The two approaches, based on examination of Figure 7, produce quite different gearing scenarios, though they both ended up deflecting the outboard surfaces (LEO, TEO) to their maximal negative values (nose-down for the leading edge, tail-up for the trailing edge). This has a tendency to shift the center of pressure inboard, thus relieving RBM (for the sequential approach) as well as strain (for the integrated approach) at the wing root. However, the two approaches differ in their use of the TEI surface, with the sequential approach using it in a negative fashion to reduce local lift forces. The integrated approach, which operates at a lower angle of attack for less loading throughout the wing, deflects the TEI all the way down (positively) so as to get more lift from the control surface.

Another interesting feature of the gearing scenario for this maneuver is that both the sequential and integrated approach deflect the horizontal tail positively. This stands in stark contrast to a conventional approach in which the horizontal tail (which is typically the only surface used for symmetric trim) is deflected in a negative manner to provide pitch-up moment to counteract the negative pitching moment produced by lift on the wing about the center of gravity. With AAW, then, the horizontal tail no longer serves to provide the pitch-up moment necessary for trim. Rather, the TEO surface, deflecting negatively, does that, and the horizontal tail carries some of the lift, thereby relieving the load on the wing.

The final gear ratios for the supersonic push-over are shown in Table 4. In this case the two approaches are very similar. This is because they have the same starting point, and since this maneuver is not a particularly critical maneuver (i.e., there are few active structural constraints associated with this maneuver) the gear ratios move little from their starting values. The characteristics of these gear ratios, though, are almost exactly the opposite of those for the subsonic pull-up. This is due to the fact that Maneuver 2 is a push-over maneuver, where the bending moments at the root are naturally negative. As a result, positive deflection of the leading edge surfaces tends to relieve load at the root, hence the positive gear ratios for these surfaces. Although the trailing edge surfaces are used heavily, their ineffectiveness at supersonic speeds results in them having little effect on the RBM, and thus they are used primarily to meet the hinge moment constraints.

Table 4 - Final Gear Ratios for Supersonic Push-Over

	Sequential	Integrated
g_{LEI2}	1.855	0.576
g_{LEO2}	1.855	2.249
g_{TEI2}	-10.870	-10.148
g_{TEO2}	5.745	1.733

Table 5 shows the final gear ratios for the supersonic roll. In this case the LEO surface is the independent surface to which the others are geared, and it deflects in a positive manner (nose-up) to produce positive roll moment. The integrated approach favors heavier usage of all of the control surfaces relative to the LEO surface as indicated by the higher gear ratios. As a result, the deflection angle of the LEO surface necessary to trim the aircraft to the steady state roll is much less for the integrated approach than the sequential. This has a tendency to more favorably distribute the load across the wing and avoid local build-ups of stress and strain that may occur in the sequential approach with its minimization of total hinge moment. Both approaches do arrive at minimal use of the trailing edge surfaces as, at supersonic speeds, these surfaces have little effectiveness.

Table 5 - Final Gear Ratios for Supersonic Roll

	Sequential	Integrated
g_{LEI3}	0.149	0.689
g_{TEI3}	0.007	0.022
g_{TEO3}	0.231	0.578

Finally, Figure 8 shows the iteration history of the gear ratio design variables for the subsonic roll, along with the corresponding final control surface deflections. As with the subsonic pull-up, both approaches arrive at significantly different solutions. Both make use of the leading edge surfaces, even though their roll effectiveness is very low at this subsonic dynamic pressure. The reason for this is that they are needed to supplement the trailing edge surfaces which have very low effectiveness due to the thin wing (3 % t/c) and the very flexible structure at the final iteration. This is also observed in the iteration history, particularly for the integrated approach, as the leading edge gear ratios increase over the course of the optimization.

The major differences between the two approaches are in how they use the trailing edge surfaces. The sequential approach actually uses the TEI surface in a reversed fashion, even though the surface's roll effectiveness is still positive, in order to alleviate hinge

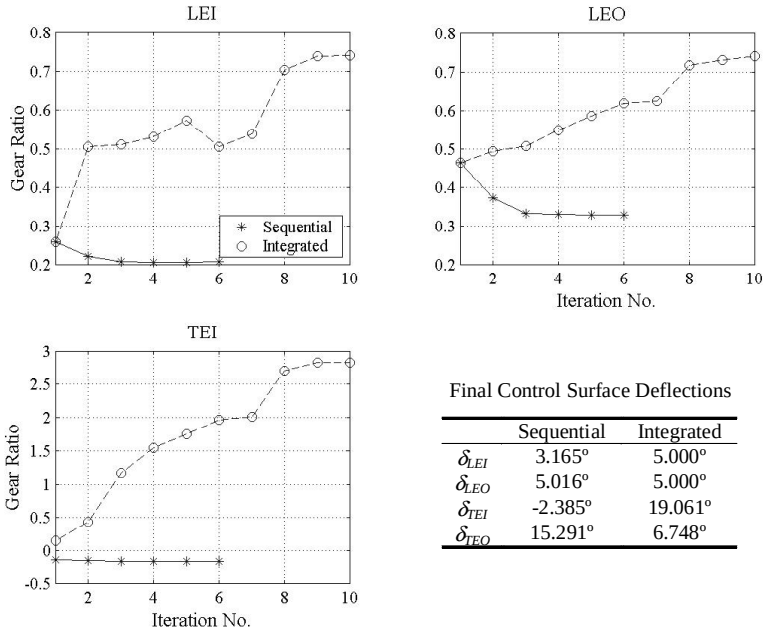

Final Control Surface Deflections

	Sequential	Integrated
δ_{LEI}	3.165°	5.000°
δ_{LEO}	5.016°	5.000°
δ_{TEI}	-2.385°	19.061°
δ_{TEO}	15.291°	6.748°

Figure 8 - Gear Ratio History – Maneuver 4

moments. The positive deflection of the TEO surface results in negative hinge moment on itself and on the TEI surface. As a result, trim optimization, with its objective of minimizing total hinge moments, pushes the TEI surface to deflect negatively, producing positive hinge moment and counteracting the negative hinge moment contribution from the TEO surface. Hence, the hinge moment of the TEI surface is negligible for this maneuver. The integrated approach favors positive deflection of the TEI surface, since it tends to relieve strain and provide increased roll moment. In fact, over the course of the optimization the integrated approach uses it increasingly more positive, even more than the TEO surface as indicated by its large gear ratio at the final iteration.

The gear ratios and control surface deflection scenarios of the four maneuvers presented above may have been somewhat different were the internal structure and/or control surfaces designed as well. This rather simplistic design study demonstrates how the different objective of the integrated and sequential approaches drive the design process into different control scenarios along with different optimized structural designs. A final, more practical, advantage of the integrated approach is that the concurrent optimization of the structure and gear ratios takes place in a single continuous run, in contrast to the sequential approach which requires pausing and restarting ASTROS, exchanging data, and performing trim optimization in a separate module. In addition, the integrated approach frees the user from selecting a trim optimization objective that may not contribute to a maximal reduction in weight.

Conclusions

A new integrated AAW design process, in which gear ratios and structural elements are simultaneously designed to minimize structural weight, is presented. The integrated approach differs from the sequential approach traditionally used for AAW design, in which trim optimization is performed separately from the structural optimization, based on an independent objective function. The integrated AAW design process is implemented in the modal-based version of ASTROS by adding the gear ratios as design variables into the optimization, and deriving and implementing the associated sensitivities and constraints.

Demonstration on a lightweight fighter design performing four symmetric and antisymmetric maneuvers has shown that the integrated approach results in trim scenarios that act to relieve strain in the wing's structural elements. This is opposed to the sequential approach which resulted in trim scenarios that support the objective that was defined for the trim optimization, which in the case of this study were the minimization of root bending moment and total hinge moment for the symmetric and antisymmetric maneuvers, respectively. Consequently, optimization using the integrated design process resulted in a lower weight structural design. In addition, the integrated approach is performed in one continuous run, thereby avoiding the pause and restart required of the sequential process.

Acknowledgments

The authors extend thanks to Prof. Moti Karpel and Dr. Boris Moulin of Technion-Israel Institute of Technology for their technical advice and programming assistance.

References

1) Miller, G.D., "Active Flexible Wing (AFW) Technology," Air Force Wright Aeronautical Laboratories, TR-87-3096, February 1988.

2) Perry III, B., Cole, S.R., and Miller, G.D., "A Summary of an AFW Program," Journal of Aircraft, Vol. 32, No. 1, January-February 1995, pp. 10-15.

3) Pendleton, E.W., Bessette, D., Field, P.B., Miller, G.D., and Griffin, K.E., "Active Aeroelastic Wing Flight Research Program: Technical Program and Model Analytical Development," Journal of Aircraft, Vol. 37, No. 4, July-August 2000, pp. 554-561.

4) Flick, P.M., Love, M.H., and Zink, P.S., "The Impact of Active Aeroelastic Wing Technology on Conceptual Aircraft Design," *Proceedings of the RTO Applied Vehicle Technology Specialists' Meeting on "Structural Aspects of Flexible Aircraft Control,"* NATO Research and Technology Agency, Ottawa, Canada, October 18-20 1999. RTO MP-36.

5) Bisplinghoff, R.L., Ashley, H., and Halfman, R.L., Aeroelasticity, Dover Publications, Inc., Mineola, New York, 1955.

6) Miller, G.D., "An Active Flexible Wing Multi-Disciplinary Design Optimization Method," 5th AIAA/USAF/NASA/ISSMO Symposium on Multidisciplinary Analysis and Optimization, Panama City, FL, September 7-9, 1994. AIAA-94-4412.

7) Volk, J. and Ausman, J., "Integration of a Generic Flight Control System into ASTROS," 37th AIAA/ASME/ASCE/AHS/ASC Structures, Structural Dynamics, and Materials Conference, Salt Lake City, UT, April 15-17, 1996. AIAA-96-1335.

8) Ausman, J., and Volk, J., "Integration of Control Surface Load Limiting into ASTROS," 38th AIAA/ ASME/ASCE/AHS/ASC Structures, Structural Dynamics, and Materials Conference, Kissimmee, FL, April 7-10, 1997. AIAA-97-1115.

9) Love, M.H., Barker, D.K., Egle, D.D., Neill, D.J., and Kolonay, R.M., "Enhanced Maneuver Airloads Simulation for the Automated Structural Optimization System – ASTROS," 38th AIAA/ ASME/ ASCE/ AHS/ ASC Structures, Structural Dynamics, and Materials Conference, Kissimmee, FL, April 7-10, 1997. AIAA-97-1116.

10) Zink, P.S., Mavris, D.N., and Raveh, D.E., "Maneuver Trim Optimization Techniques for Active Aeroelastic Wings," AIAA/ASME/ASCE/AHS/ASC Structures, Structural Dynamics, and Materials Conference, Atlanta, GA, April 3-6, 2000. AIAA-2000-1330.

11) Zillmer, S., "Integrated Multidisciplinary Optimization for Active Aeroelastic Wing Design," Air Force Wright Aeronautical Laboratories, WL-TR-97-3087, August 1997.

12) Dobbs, S.K., Schwanz, R.C., and Abdi, F., "Automated Structural Analysis Process at Rockwell," *Proceedings of the 82nd Meeting of the AGARD Structures and Materials Panel on "Integrated Airframe Design Technology*," Sesimbra, Portugal, May 8-9 1996. AGARD Report 814.

13) Rodden, W.P., and Johnson, E.H., MSC/NASTRAN Version 68 Aeroelastic Analysis User's Guide, The Macneal-Schwendler Corporation, 1994.

14) Neill, D.J., Johnson, E.H., and Canfield, R., "ASTROS-A Multidisciplinary Automated Design Tool," Journal of Aircraft, Vol. 27, No. 12, 1990, pp. 1021-1027.

15) Zink, P.S., Mavris, D.N., Flick, P.M., and Love, M.H., "Impact of Active Aeroelastic Wing Technology on Wing Geometry using Response Surface Methodology," CEAS/AIAA/ICASE/NASA Langley International Forum on Aeroelasticity and Structural Dynamics, Williamsburg, VA, June 22-25, 1999.

16) Zink, P.S., Mavris, D.N., Flick, P.M., and Love, M.H., "Development of Wing Structural Weight Equation for Active Aeroelastic Wing Technology," SAE/AIAA World Aviation Congress and Exposition, San Francisco, CA, October 19-21, 1999. SAE-1999-01-5640.

17) Dantzig, G.B., Orden, A., Wolfe, P., "The Generalized Simplex Method for Minimizing a Linear Form under Linear Inequality Restraints," Pacific Journal of Mathematics, Vol. 5, 1955, pp. 183 – 195.

18) Karpel, M., Moulin, B., and Love, M.H., "Modal-Based Structural Optimization with Static Aeroelastic and Stress Constraints," Journal of Aircraft, Vol. 34, No. 3, 1997, pp.433-440.

19) Karpel, M., "Modal-Based Enhancement of Integrated Design Optimization Schemes," Journal of Aircraft, Vol. 35, No. 3, 1998, pp. 437-444.

20) Vanderplaats, G.N., "An Efficient Feasible Directions Algorithm for Design Synthesis," AIAA Journal, Vol. 22, No. 11, November 1984, pp. 1633 – 1640.

21) Karpel, M., "Modal-Based Structural Optimization using ASTROS-Theoretical Manual," Technion-Israel Institute of Technology, Haifa, Israel, September 1997, TAE No. 795 (Supported by Lockheed Martin Tactical Aircraft Systems, Ft. Worth, TX).

22) Johnson, E.H., and Venkayya, V.B., ASTROS Theoretical Manual, AFWAL-TR-88-3028, December 1988.

23) Rodden, W.P., and Love, J.R., "Equations of Motion of Quasisteady Flight Vehicle Utilizing Restrained Static Aeroelastic Characteristics," Journal of Aircraft, Vol. 22, No. 9, September 1995, pp. 802–809.

24) Zink, P.S., Mavris, D.N., and Raveh, D.E., "Integrated Structural/Trim Optimization for Active Aeroelastic Wing Technology," 8th AIAA/NASA/USAF/ISSMO Symposium on Multidisciplinary Analysis and Optimization, Long Beach, CA, Sept. 6-8, 2000. AIAA-2000-4827.

25) MathWorks, Inc., Using MATLAB – Version 5, 1996.

26) Chvátal, V., Linear Programming, W.H. Freeman and Company, New York, 1983, p. 222.

27) Zink, P.S., Mavris, D.N., Love, M.H., and Karpel, M., "Robust Design for Aeroelastically Tailored/Active Aeroelastic Wing," 7th AIAA/USAF/NASA/ISSMO Symposium on Multidisciplinary Analysis and Optimization, St. Louis, MO, September 2-4, 1998, AIAA-98-4781.

28) Carmichael, R.L., Castellano, C.R., and Chen, C.F., The Use of Finite Element Methods for Predicting the Aerodynamics of Wing-Body Combinations, NASA SP-228, October 1969.

29) Barker, D.K. and Love, M.H., "An ASTROS Application with Path Dependent Results," AIAA/USAF/NASA/ISSMO Multidisciplinary Analysis and Optimization Conference, Bellevue, WA, September 1996.